1 Model explainability and physical connections

This section aims at presenting results intended to explain aspects of the deep learning system, such as predictor importance, how the model responds to the predictors as well as understanding how decisions where made by the deep learning system. This will be divided into three subsections. Firstly, model response to modified predictors will be measured. Secondly, individual predictions will be used to highlight how the model interprets the input data for decision-making. Thirdly, a case study will be conducted with the intent to relate the previous explainability results to a real world and in-distribution scenario.

1.1 Predictor importance

To measure the impact of each predictor, an experiment was conducted where the deep learning system was fitted to subset of the predictors, and the Normalized IIEE with respect to the ($\geq 10\%$) contour was measured as a yearly mean value. The result of the experiment can be seen in Figure 1, where also persistence as well as an all predictor baseline was included for reference. From figure 1, it can be seen that removing the recent sea ice chart as a predictor causes the deep learning system to achieve the highest NIIEE. Moreover, only when removing all AROME Arctic atmospheric predictors does the deep learning system perform worse than persistence for the 2022 test data period. Finally, removing t2m seem to stochastically improve the forecast beyond the baseline with all predictors, as further indicated by training a new model without t2m which achieves similar performance (orange line).

Moreover, two more experiments where conducted to explore how sensitive a model fitted to all parameters are to perturbations in the input data. Firstly, it is noted that the model is trained on unaltered training and validation data, only the test dataset is permuted. The first experiment involves swapping all predictors with uniform noise between 0 and 1, which is the value range for the predictors after normalization (see section 1.1.6). The purpose of replacing a predictor with a uniform noise field is to study how much it alters the prediction of the model, i.e. if the model is strongly fitted to the predictor. The result of the first experiment is seen in figure 2, and although not shown permuting SIC results in the values [383, 439, 870, 851] following the same seasonal sequence as figure 2.

Inspecting figure 2 reveals that permuting SIC results in the highest NIIEE seasonal means. Following SIC, when swapping temperature out with random uniform noise, the NIIEE seasonal means are higher then persistence for both JJA and SON.

The second experiment conducted is similarly constructed to the previously described experiment of swapping out predictors with random noise, however instead of replacing each predictor with random noise each predictor have their 2022 test dataset sequence
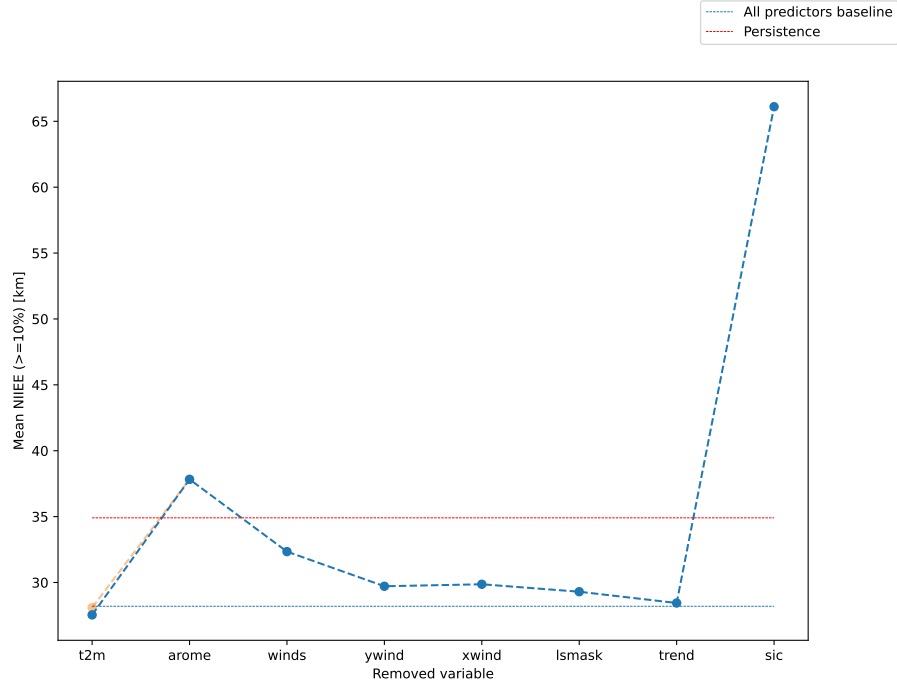
Figure 1: Yearly mean NIIEE for the (≥ 10%) contour computed for deep learning systems where one (or a group) of the predictors have been removed. The red dashed line denotes the yearly mean NIIEE computed from persistence, whereas the blue dashed line denotes the yearly mean NIIEE for a benchmark deep learning model with all predictors. A two day lead time was considered. The orange mark and line seen for t2m is from an independent rerun. Trend refers to the OSI SAF linear sea ice trend. Winds refer to removing both the x and y component of the wind, whereas arome means removing all AROME Arctic atmospheric predictors.
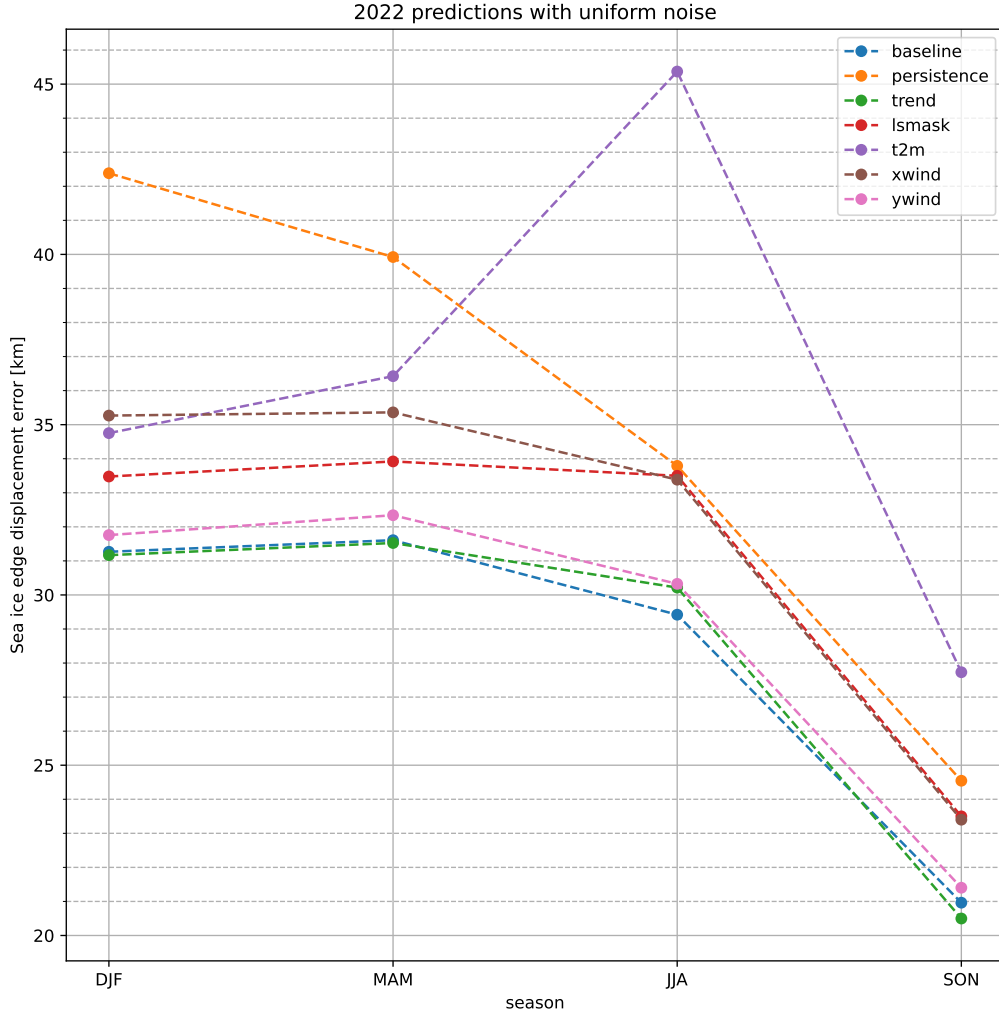
Figure 2: Seasonally distributed mean NIIEE for the ($\geq 10\%$) contour where each of the predictors have been swapped out with uniform noise between 0 and 1. Each colored line represent a variable that has been replaced, however the blue and orange line represent a no permuted baseline and persistence respectively. SIC is not shown, as it achieves the values [383, 439, 870, 851] distributed in the same seasonal sequence as the shown lines.

swapped. Thus, the distribution in which samples are drawn from is preserved. To account for seasonality, each prediction on the test data was repeated ten times for each predictor. The results of swapping predictor fields with fields from a different date is seen in figure 3. As with figure 2, SIC is not shown but achieves the values $[186 \pm 13, 225 \pm 29, 266 \pm 36, 230 \pm 29]$ distributed in the same seasonal sequence as in figure 3.

From figure 3, it can be seen that swapping t2m is the only predictor which achieves a significantly higher NIIEE than persistence for the months JJA and SON. Moreover, for all seasons, all AROME Arctic predictors cause the model to have significantly higher NIIEE than the non-AROME Arctic predictors for all seasons. Figure 3 also shows that the swapped OSI SAF trend exerts no discernable standard deviation at all seasons.

1.2 Synthetic AROME Artcic fields

Following the predictor importance experiments described previously in section 1.1, this section will describe an experiment which only targets the atmospheric predictors provided by AROME Arctic by constructing synthetic atmospheric fields and measuring how the deep learning system reacts. Firstly, a brief rundown of the synthetically created AROME Arctic fields and the experiment environment will be provided.

The deep learning model chosen is, similar to previous results, a model trained on all predictors with a two day lead time. Four prediction dates covering months from different seasons have been chosen when measuring how the model responds to artificial AROME Arctic data, with the intent to also measure any seasonal variability in the responses. The chosen dates were 03rd March, 03rd June, 07th September and 07th December, with the dates referring to the valid date of the forecasts. Moreover, different synthetic fields were created.

With regards to temperature, four fields were created where temperature increases linearly from one end of the domain to the other, starting at the lowest possible t2m value in the test dataset and ending at the maximum t2m value in the test dataset. Moreover, two homogenous fields containing only minimum or maximum values were created. For the winds, seven different fields were set up. The first field contains no wind in either x or y direction. Additionally, four fields where the wind blew in one direction (x or y, as well as positive or negative) where created. Finally, two fields were the winds were set to their maximum and minimum value in x and y at the same time was initiated.

Figure 4 show how the model respond to synthetic AROME Arctic fields in terms of the NIIEE computed at the $(\geq 10\%)$ contour. From the figure, it can be seen that the model respond differently to the different fields for the inspected seasons. The synthetic fields tend to give the deep learning system higher NIIEE, except for two wind related fields for the september prediction. For all seasons, the highest NIIEE value is achieved with
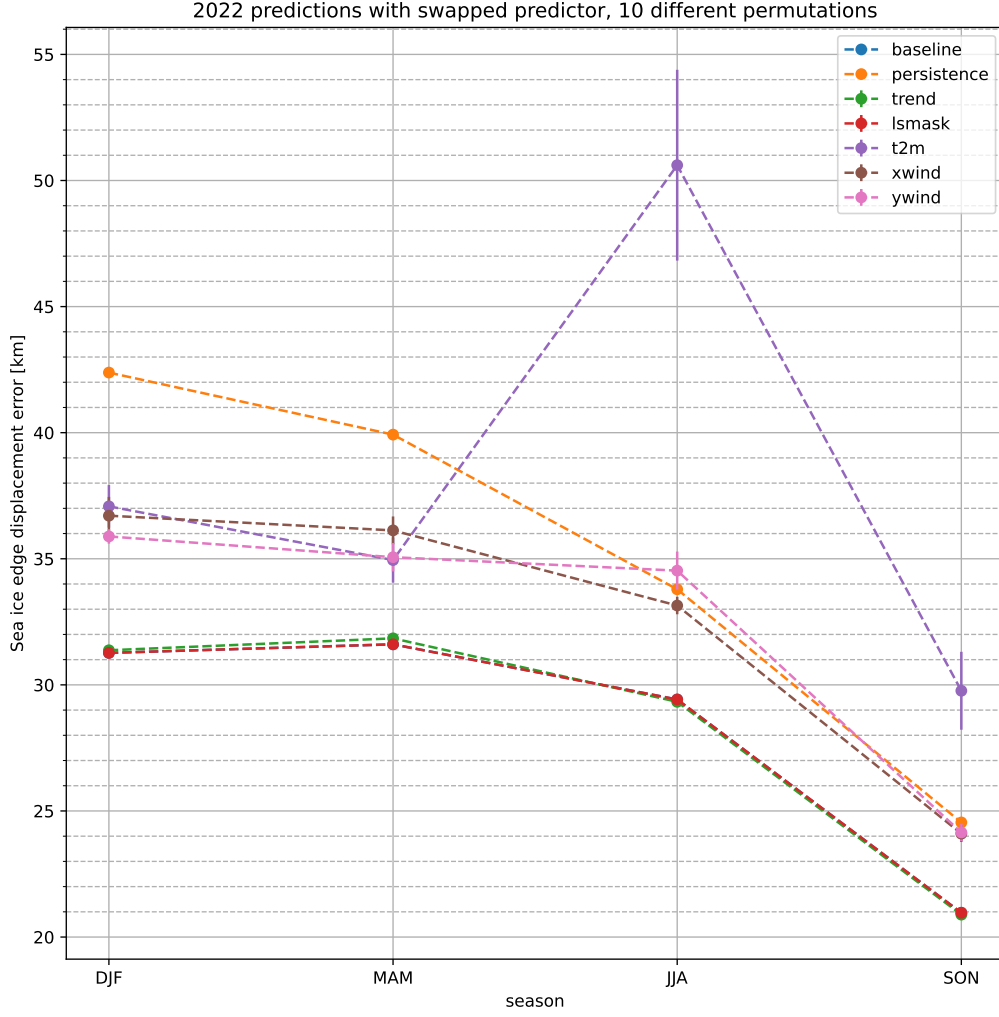
4

Figure 3: Seasonally distributed mean NIIEE for the ($\geq 10\%$) contour across 10 runs for each predictor, where each predictor have had their fields swapped internally. Each line represents one predictor. SIC is not shown, but it achieves the values $[186 \pm 13, 225 \pm 29, 266 \pm 36, 230 \pm 29]$.
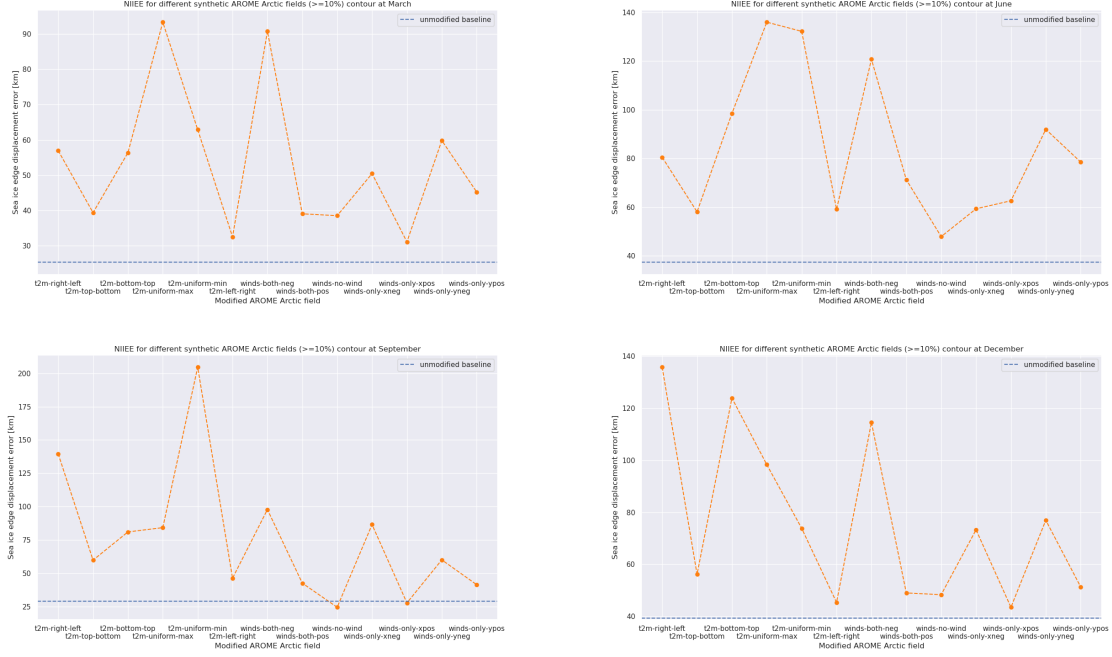
Figure 4: NIIEE across different synthetic AROME Arctic fields measured at the ($\geq 10\%$) contour for different seasons. The deep learning system has a two day lead time. The blue dashed line show the NIIEE value for a baseline model with no synthetic AROME Arctic field. The x axis describe how the different field were created.

a synthetic temperature field, although having both the x and y winds at a maximum negative direction causes the highest NIIEE for all seasons compared to the other synthetic wind fields.

Spatial errors are shown in figure 5, where some of the predictions made with the synthetic fields have been chosen. The top row of figure 5 show two examples where synthetic wind fields have been constructed, and it is noted that a negative y-wind direction is towards the top of the domain. When both wind fields are pointed in a negative direction with maximum velocity from the test set, the sea ice concentration rend towards lower categories as seen by the negative difference along the sea ice edge. With only x-wind in the positive direction with a maximum test set magnitude, a varied distribution of differences occur along the sea ice edge, with an overall weak signature.

The lowermost row contain two prediction differences made with synthetic t2m. The lower leftmost figure show a consistent increase in sea ice concentration when the entire domain is covered by the lowest t2m value found in the test dataset. Sea ice is forming in areas where it is usually not found during September, and sea ice is also forming along the coast of Norway. A similar response can be seen in the December prediction to the lower right,

6

where temperature is linearly increasing from the minimum to maximum value of the test dataset form the bottom of the domain to the top of the domain. Sea ice is forming along the lower border of the domain, as well as above Russia. Moreover, following the temperature gradient, the sea ice tend to decrease as the t2m increases. With the topmost past of the domain experiencing consistent melting.

1.3   Understanding predictions

Sections 1.1 and 1.2 have presented results which attempt to explain the relationship between model performance and predictors. In the current section, predictions will be used to explain model decision-making through the use of segmentation gradient class activation maps (seg-GradCAM) (Vinogradova et al., 2020) which was presented and described in section 1.6.1. Due to the formulation of the targets as cumulative contours (section 1.1.5), the gradient has to be computed from a single target output contour. Thus, each seg-GradCAM will only contain information related to wether a pixel was important for predicting the chosen cumulative contour, as a network used to create a segmentation gradient class activation map will be limited to predict only one cumulative contour.

When creating seg-GradCAMs, only the final layer of the encoder will be considered following the recommendations made by Vinogradova et al. (2020). This approach is also compliant with the originally proposed gradient class activation mapping (GradCAM) for classification tasks (Selvaraju et al., 2016), where it is recommended to compute the gradient with respect to the final convolutional layer. Since neither GradCAM or seg-GradCAM is intended for quantitative analysis, nor are there any studies known to the author where the methods have been applied to compute statistics, a case study approach is adopted where seg-GradCAMs from varying dates and contours will be inspected and compared. To experiments are conducted, one where the baseline model is compared against the model with reduced classes at different contours, and one where the baseline model is compared against the model trained without 2-meter temperature. For the first experiment where target contours are varied, 5th of January 2022 is chosen as the target date. For the second experiment where dates are varied. the same dates as those used in the synthetic AROME Arctic fields experiments are chosen, namely 03rd March, 03rd June, 7th September and 7th December.

For all the following figures, a shared colorscale is used as values have been normalized between 0 and 1 following Vinogradova et al. (2020). However, the actual values are not comparable, hence each seg-GradCAM visualizes the relative importance of each pixel for each contour. Furthermore, although Vinogradova et al. (2020) presents seg-GradCAM as a GradCAM computed from an arbitrary region of interest, for the following experiments the region of interest was defined as all pixels classified as part of the cumulative contour (both true and false positives). Furthermore, only non-zero values are shown.
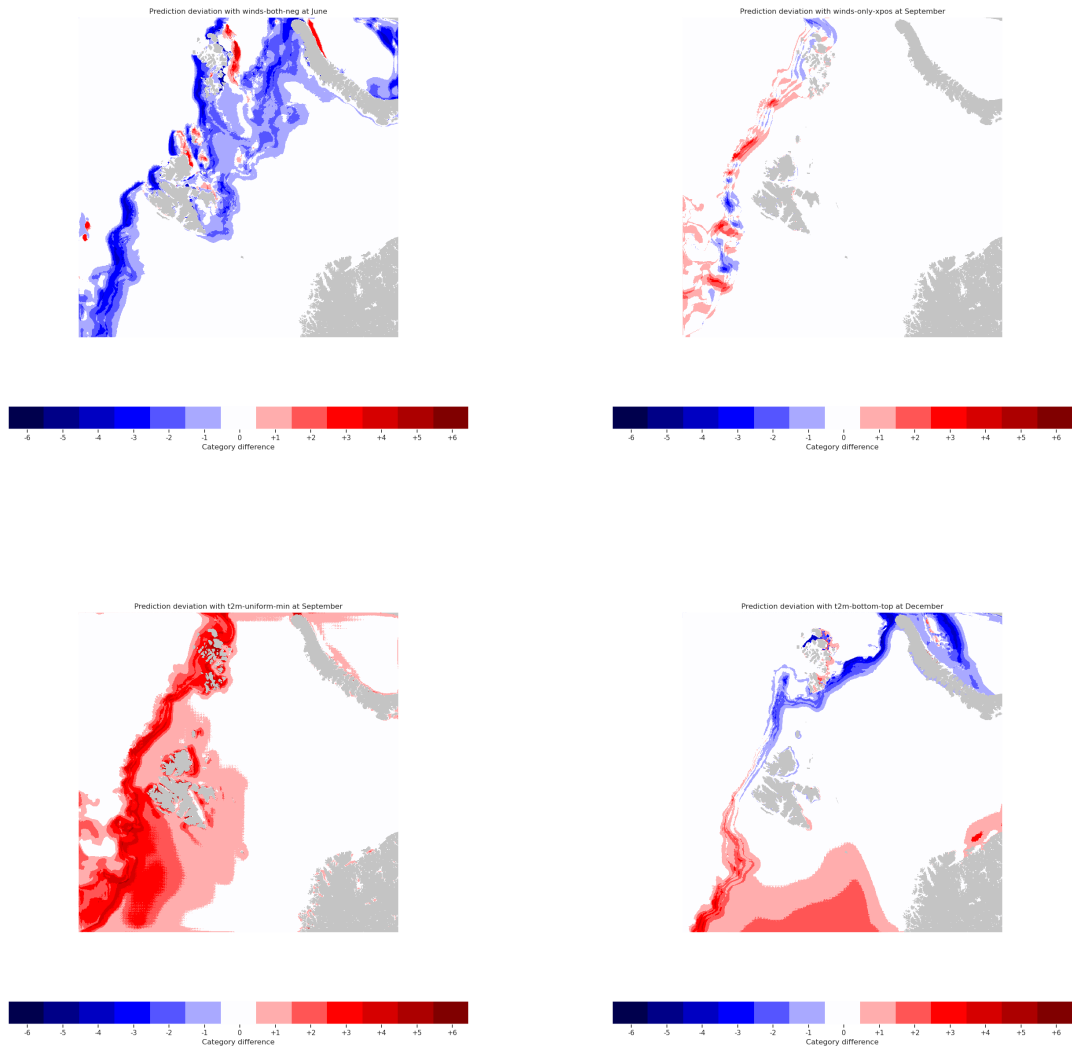
Figure 5: Sea ice contour error with respective to the baseline prediction with no synthetic AROME Arctic field. The figure show a selection of the synthetic fields, with the purpose of visualizing spatially how the deep learning system responds.
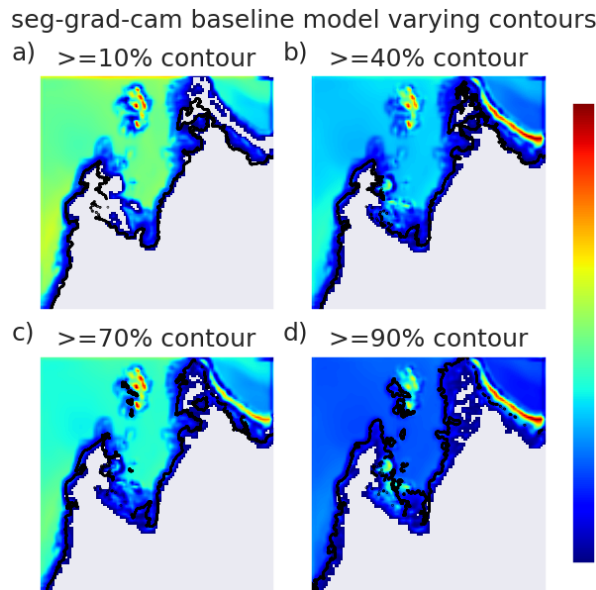
Figure 6: Segmentation class activation maps for varying target contours for the same date. The model used is the baseline model predicting with a two day lead time. The black line is the sea ice edge for the relevant contour from the input sea ice chart.

A seg-GradCAM for varying target contours for the baseline model with a two day lead time is shown in figure 6. The maps are spatially similar, although the intensity of the activated features tend to vary without a clear trend. The activated features seem to closely resemble the position of the sea ice edge. For figure 6 (a, b, c and d) the features with highest activation seem to be located in Frans Josef Land and Novaya Semlya (the latter not for (a)).

The seg-GradCAMs for the model without the $< 10\%$ and $= 100\%$ / fast-ice contour is shown in figure 7. Each seg-GradCAM in figure 7 has significantly higher relative values compared to figure 6. Moreover, whereas the highest activation values occurred over Frans Josef Land and Novaya Semlya for figure 6, the opposite seems to be the effect for figure 7. Furthermore, some spurious activations occur in figure 7 (a, b, c) located towards the lower right where mainland Norway is located.

The varying dates experiment for the baseline model is shown in figure 8. As with figure 6, the activated features tend to follow the sea ice edge, with no activated pixels located significantly outside of the sea ice edge. The relative value tend to be towards the upper limit, especially for figure 8 (b, c and d).

Finally, seg-GradCAM from the model trained without 2-meter temperature is shown in

seg-grad-cam reduced classes varying contours

a) >=10% contour b) >=40% contour

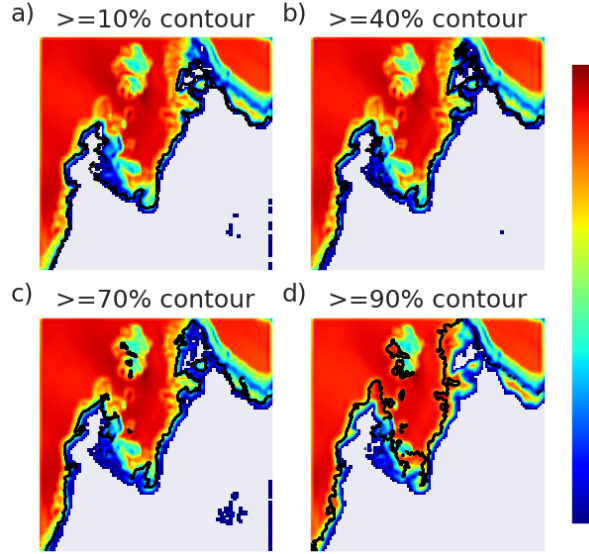c) >=70% contour d) >=90% contour

Figure 7: Segmentation class activation maps for varying target contours for the same date. The model used is the reduced classes model predicting with a two day lead time. The black line is the sea ice edge for the relevant contour from the input sea ice chart.

seg-grad-cam baseline model varying dates

a) 3rd March b) 3rd June
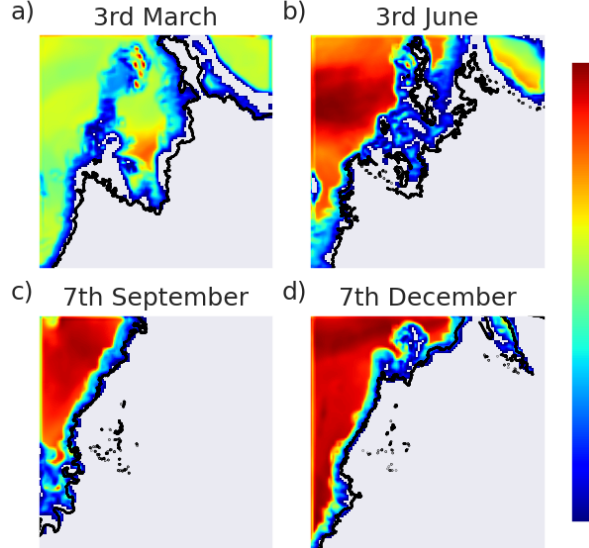
c) 7th September d) 7th December

Figure 8: Segmentation class activation maps for varying dates for the same target contour. The model used is the baseline model predicting with a two day lead time. The black line is the sea ice edge for the relevant date from the input sea ice chart.

seg-grad-cam w.o. t2m varying dates

a) 3rd March   b) 3rd June
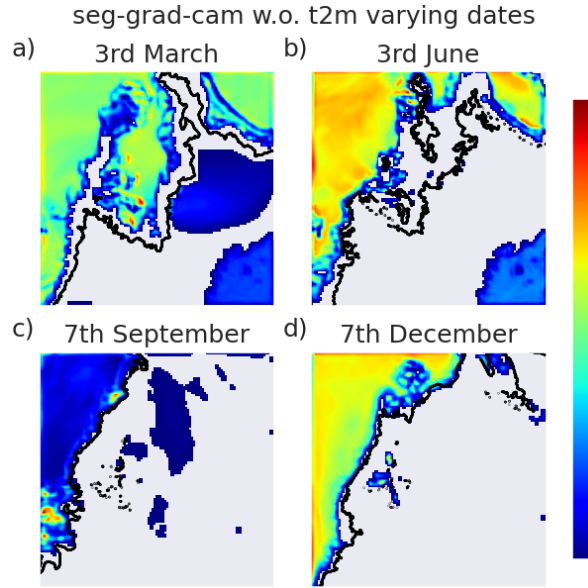
c) 7th September   d) 7th December

Figure 9: Segmentation class activation maps for varying dates for the same target contour. The model used is a model without 2-meter temperature as a predictor predicting with a two day lead time. The black line is the sea ice edge for the relevant date from the input sea ice chart.

figure 9. Compared to figure 8, the relative values tend towards lower values. Contrary to figure 8, figure 9 contain several large patches of activated features with low values located outside the border of the sea ice edge. For figure 9 (a and b), features located under Norway have been consistently activated. Moreover, for figure 9 (d) there appears to be activated features located in the inlet fjords of Svalbard, which is not seen in figure 8 (d).

Mean 2-meter temperature fields from AROME Arctic, used as predictors for the baseline model used in figure 8. The sea ice chart is included to highlight the temperature-gradient in the scenes.

Kanskje i appendix

1.4 Case study

A case study is conducted for the date with the highest reported IIEE value from the baseline machine learning model, with a two day lead time. The motivation behind presenting a case study is to relate the previous model explainability results in sections 1.1 and 1.2 to an example where the predictors are in-distribution, thus representing a possible model prediction. The day chosen was 18th of March 2022 (valid date), which implies that the deep learning forecast was initialized 16th of March 2022 (bulletin date). For the current
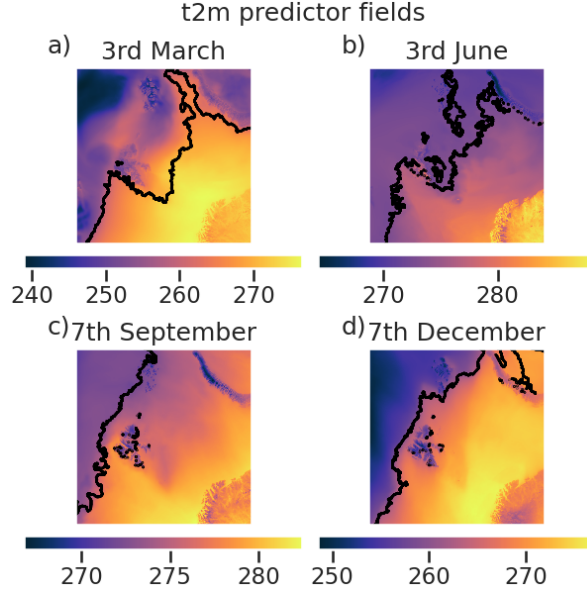
Figure 10: 2-meter temperature mean fields used as predictor for the baseline model for varying dates. The black line is the sea ice edge for the relevant date from the input sea ice chart.

date, the deep learning forecast achieved an NIIEE of 50.8km, with persistence achieving an NIIEE of 52.5km for the same date. The chosen date is 14th highest persistence NIIEE value. The purpose of including a case study is understand if connections can be drawn between the input variables and output forecast, with the date of highest NIIEE for the test dataset chosen as it may be characterized by outlier like conditions compared to the mean annual NIIEE for the baseline model (28.2km). We believe that discussing an outlier prediction is instructive in terms of model explainability, as it may provide further insight into how the model responds to the input predictors. Furthermore, exploring the lower limits of model performance may reveal sea ice conditions in which the model is not well suited to predict.

The sea ice conditions for the bulletin and valid date, as well as the sea ice forecast for the valid date is visualized in figure 11. To aid in visualizing the differences between the sea ice concentration fields, the 10% sea ice edge from the bulletin (figure 11 (a)) is visualized in figure 11 (a, b and c). The sea ice edge for the valid sea ice field is only shown in figure 11 (c) as the blue line. The two sea ice edges closely match along MIZ, however a major deviation between the two dates is the occurrence of a major loss of $10 - 30\%$ sea ice north east of Svalbard for the bulletin date sea ice chart (figure 11 (b)). It is seen in figure 11 (c) that the deep learning forecast has not predicted this particular loss of sea ice. For clarity, the sea ice chart in figure 11 (a) was used as input for the deep learning system to make the forecast seen in figure 11 (c).
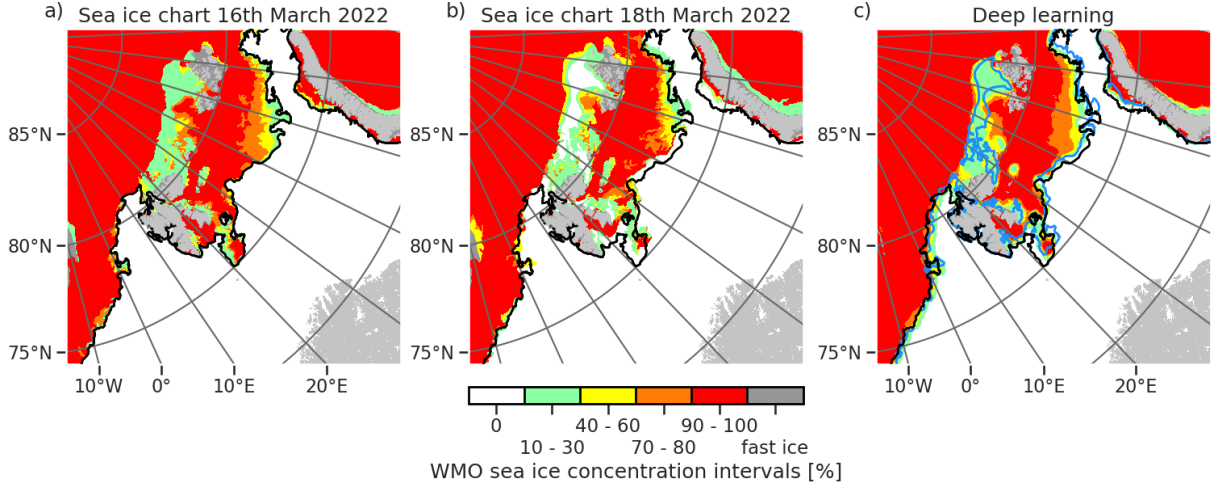
Figure 11: Sea ice charts for the 16th (a) and 18th (b) of March 2022, with a deep learning prediction for 18th of March 2022 initialized 16th of March 2022 in (c). The black line is the sea ice edge for the sea ice chart in (a) and blue line is the sea ice edge for the sea ice chart in (b), both are thresholded by 10% sea ice concentration. The < 10% sea ice concentration contour is not shown.

The atmospheric predictors used to make the forecast in figure 11 (c) are given in figure 12. The fields shown are 2-meter temperature, as well as the x and y wind, which have been computed as two day mean fields between 16th of March 2022 18:00UTC and 18th of March 2022 12:00UTC following the approach for atmospheric predictor construction described in section 1.1.4. The 2-meter temperature field contains values ∼ 273K, although significantly lower values are seen towards the top left of the scene (figure 12 (a)). The x-wind field mostly contain values centered about 0 m/s, although some outlier values are located along the north of Novaya Semlya blowing strongly towards the left of the scene (figure 12 (b)). The y-wind component show that the winds vary between blowing towards the top and bottom of the domain, although the y-wind along the sea ice edge (MIZ) tend to be directed towards the bottom of the domain (figure 12 (c)).

The spatial distribution of deep learning forecast sea ice concentration overestimation and underestimation (Goessling et al., 2016) with respect to the valid date sea ice chart is shown in figure 13. Furthermore, areas where the two products agree are denoted as sea ice (for positive agreement) and Ocean (negative agreement). The land sea mask is included in figure 13, as the IIEE is computed sans the land pixels. The deep learning forecast unresolved lack of sea ice north east of Svalbard (figure 11 (c)) is clearly shown as overestimated sea ice concentration in figure 13. Furthermore, figure 13 show that the sea ice edge along the MIZ is overestimated towards the bottom of the domain, with some spurious overestimation located south of Svalbard. A consistent overestimation occurs
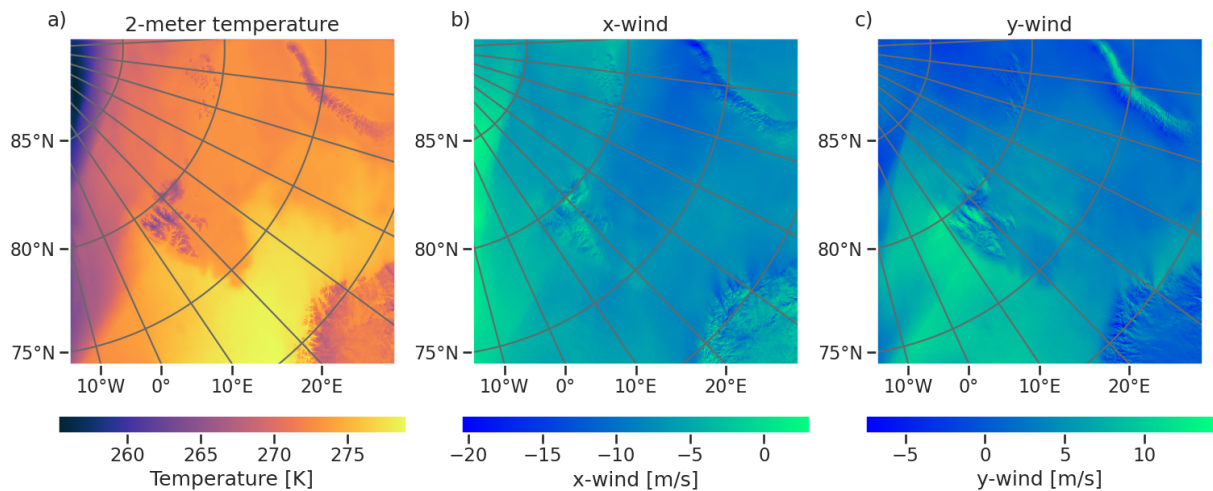
13

Figure 12: Atmospheric predictors for a sample initialized 16th of March 2022 for a two day lead time model. (a) is the two day mean AROME Arctic 2-meter temperature field. (b) and (c) are the two day mean x and y wind fields from AROME Arctic respectively.

towards the top of the domain, at the sea ice edge located opposite the northern edge of Novaya Semlya. Contrary, the sea ice concentration is overestimated along the coast of Novaya Semlya.

References

Goessling, H. F., Tietsche, S., Day, J. J., Hawkins, E., and Jung, T.: Predictability of the Arctic sea ice edge, Geophysical Research Letters, 43, 1642–1650, https://doi.org/10.1002/2015gl067232, 2016.

Selvaraju, R. R., Cogswell, M., Das, A., Vedantam, R., Parikh, D., and Batra, D.: Grad-CAM: Visual Explanations from Deep Networks via Gradient-based Localization, International Journal of Computer Vision, 128, 336–359, https://doi.org/10.1007/s11263-019-01228-7, 2016.

Vinogradova, K., Dibrov, A., and Myers, G.: Towards Interpretable Semantic Segmentation via Gradient-Weighted Class Activation Mapping (Student Abstract), Proceedings of the AAAI Conference on Artificial Intelligence, 34, 13 943–13 944, https://doi.org/10.1609/aaai.v34i10.7244, 2020.
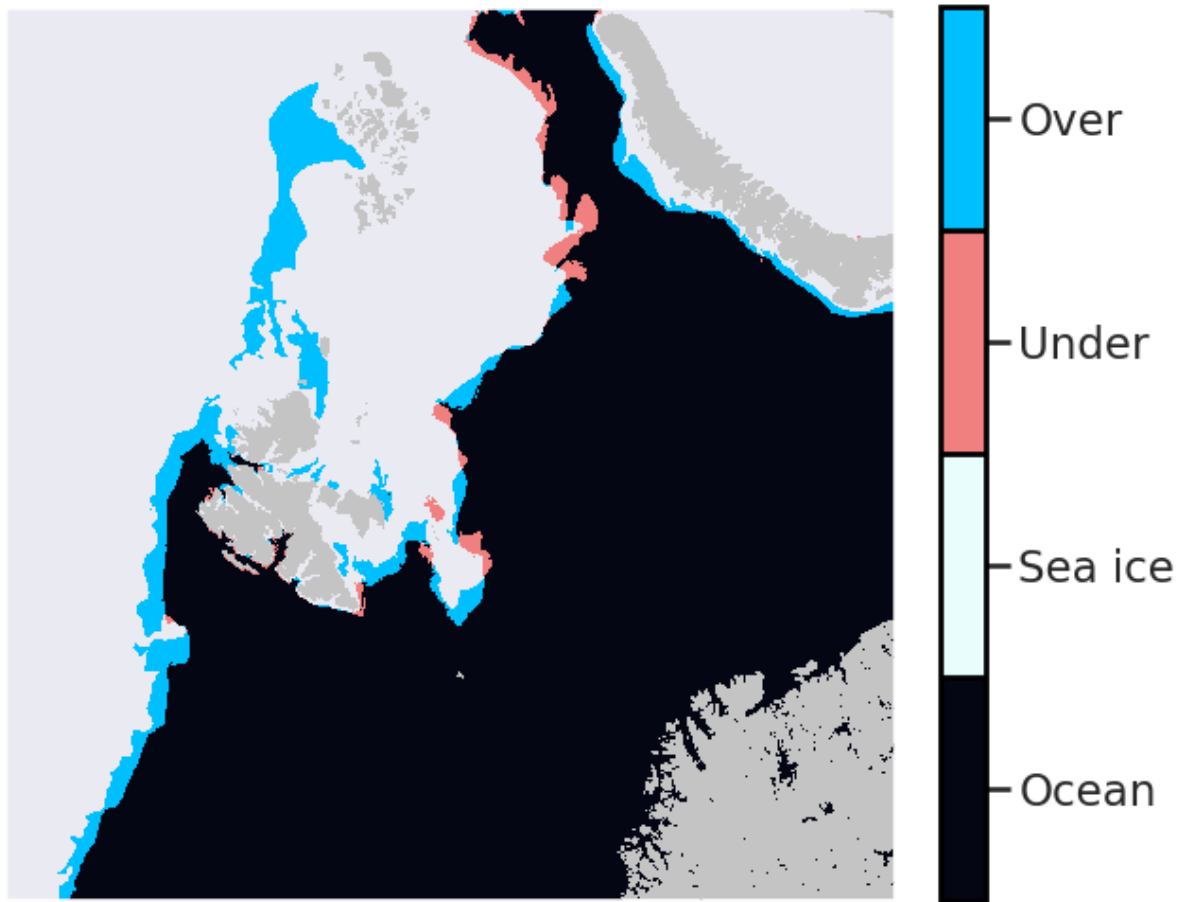
Figure 13: IIEE computed between the deep learning forecast valid 18th of March, initialized 16th of March 2022 and the sea ice chart for 18th of March 2022. Sea ice and Ocean denote true positives and true negative for the deep learning forecast.